Chemical Engineering Journal 146 (2009) 466–476

Contents lists available at ScienceDirect

Chemical Engineering Journal

journal homepage: www.elsevier.com/locate/cej

Steady-state particle size distribution modeling of polypropylene produced in tubular loop reactors

Zheng-Hong Luo*, Pei-Lin Su, Xiao-Zi You, De-Pan Shi, Jin-Cheng Wu

Department of Chemical and Biochemical Engineering, College of Chemistry and Chemical Engineering, Xiamen University, Shiming Street 422, Xiamen 361005, People's Republic of China

ARTICLE INFO

Article history:
Received 31 July 2008
Received in revised form 23 October 2008
Accepted 26 October 2008

Keywords:
Polypropylene
Tubular loop reactor
PSD
Population balance
Steady state

ABSTRACT

A comprehensive steady-state population balance model is developed for the particle size distribution (PSD) of the polypropylene produced in tubular loop reactors. The model considers the flow type, the polymer particle dynamics, the particle growth and the attrition. Moreover, an empirical single particle model is used to describe the particle growth under internal and external heat and mass transfer limitations totally. The predicted PSD data obtained under steady-state polymerization conditions agree well with the actual data collected from industrial scale plant. The model are also used to predict the effects of some operational parameters on the polymer PSD produced under steady-state conditions. The results show that the polymer PSD are greatly affected by the feed catalyst size, the feed catalyst PSD, and the polymerization temperature.

1. Introduction

Polypropylene can be produced in various types of reactors, such as autoclave, continuous stirred tank, fluidized-bed reactor (FBR) or tubular loop reactor. The last one is certainly the most important at present [1]. In the tubular loop reactor, small catalyst particles (e.g. 20–100 μm) react with monomers to form polymer particles in a size range of 100–5000 μm in a liquid phase and the polymer particles are produced as a solid suspension in the liquid stream [2–8]. In addition, the polymerization rate, the cost of post-treatment after polymeric process and the polymer properties are influenced by the polymer particle size distribution (PSD) [6–8]. Therefore, the polymer PSD modeling may be useful for the understanding of the propylene polymerization in tubular loop reactors. Furthermore, a mathematical model is necessary in order to predict the effects of operation parameters, especially the feed catalyst on the product PSD in tubular loop reactors.

In propylene polymerization field, most of papers published were concerned with the modeling of heat and mass transfer inside the polymer particles and of the reaction mechanism [9–12]. The overall polymerization process combined with the polymer PSD in the reactor was usually neglected.

Choi et al. [13] put forward a population balance model for a continuous gas-phase olefin polymerization reactor. The model predicted the effects of the feed catalyst PSD on the polyolefin PSD produced in a FBR. Soares et al. [14] developed a mathematical model to analyze the effects of the ideal and non-ideal reactor residence time distributions on the polymer PSD. Zacca et al. [2] presented a population balance approach modeling of multistage olefin polymerization processes using the catalyst residence time as main coordinate. Their work allowed the consideration of particle size selection effects within the process in a FBR. Khang et al. [3] developed a population balance approach to model the effect of non-ideal mixing behavior of solid particles on the polyolefin PSD in a FBR. Hatzantonis et al. [4] developed a generalized steady-state population balance model rigorously accounting for the combined effects of particle growth, attrition, elutriation and agglomeration in a gas-phase FBR. Yiannoulakis et al. [5] employed a polymeric flow model to describe the growth rate of a single particle under internal and external heat and mass transfer limitations in a FBR and this single particle model was solved together with a steady-state population balance model to predict polymer PSD. Mattos et al. [15] developed and implemented a mathematical model for steady-state slurry and bulk propylene polymerization process. The model was capable of predicting the polymer molecular structure and morphology, including PSD. Using a mixing cell approach and detailed polymerization kinetics combined with population balance equation, Harshe et al. [6] developed a comprehensive model for propylene polymerization in a FBR. The need for coupling the reaction-engineering model with the population balance equation was also demonstrated in their work.

* Corresponding author. Tel.: +86 592 2187190; fax: +86 592 2187231.
E-mail address: luozh@xmu.edu.cn (Z.-H. Luo).

1385-8947/$ – see front matter © 2008 Elsevier B.V. All rights reserved.
doi:10.1016/j.cej.2008.10.023

Nomenclature

A	parameter for the fine powders' size distribution
C^*	concentration of activate site (mol/kg)
D	particle diameter (m)
$E(t)$	residence time density function (h^{-1})
F	flowrate (kg/h)
$F(t)$	residence time accumulation function
$G(D)$	particle diameter growth rate (m/h)
k	reaction kinetic constant
m	particle mass (kg)
M	monomer concentration (mol/m^3)
M_m	monomer molecular weight (kg/mol)
n	parameter for single particle model
$P(D)$	mass density function (m^{-1})
r	reaction rate
R_a	particle diameter attrition rate (m/h)
t	residence time (h)
T	reaction temperature (°C)
w	weight fraction of solid phase in the reactor
W	total particles mass in tubular loop reactor (kg)

Greek letters and symbols

η	efficiency
π	mathematical constant
ρ	particle density (kg/m^3)
σ	standard deviation

Subscripts and superscripts

cat	catalyst property
d	deactivation reaction
DONOR	electronic donor for Ziegler–Natta catalyst
e	efficiency
f	polymer fine powders
H_2	hydrogen
max	maximum size
min	minimum size
p	propagation reaction
pp	polypropylene
prop	propylene
TEAL	triethyl aluminum
0	initial stage
1	inlet stream
2	outlet stream
200	prepolymerization reactor R200
201	main polymerization reactor R201

Based on above discussion, it becomes clear that the early modeling efforts in this field are made to account for the detailed aspect of the population balance model and the particle residence time in reactors separately. In practice, the two are coupled with each other. It is also clear that the PSD models established before mainly focused on the FBR. Though there is no difference between them when both FBR and tubular loop reactor are treated as a continuous stirred tank reactor (CSTR) in simulation, they are still different in plant operation and solution methodology of the population balance equation. Moreover, it is important that most of the PSD models proposed are not validated with any actual industrial data. Nevertheless, they are still helpful as reference when dealing with the PSD model of the polypropylene produced in tubular loop reactors.

In the present work, a comprehensive steady-state population balance model is developed for the prediction of the polypropylene PSD produced in the tubular loop reactors. Based on the reaction parameters estimation and the population balance equation, the model takes into account the flow type, the particle dynamics and the particle growth, as well as, the attrition. Particular attention is paid to the effects of the operational parameters on the polymer PSD and to the comparison of PSD between the predicted and the actual data.

2. Process for propylene polymerization in tubular loop reactors

In the present study, Himont Spheripol Loop technology with the continuous tubular loop reactors as its heart is studied. To illustrate the concepts discussed in this paper, a typical schematic flow sheet is given in Fig. 1.

There are many papers concerning the loop technology [2,16,17]. Comprehensive reviews have also been reported [18,19]. Some points related to this work are listed in the following contents. First, the loop reactors, including the prepolymerization reactor (R200, 0.46 m^3) and the main polymerization reactor (R201, 56 m^3), are of most importance in the Himont Spheripol Loop technology. Secondly, R201 consists of three tubular reactors connected in sequence with each other, in practice, the tubular loop reactor is a closed tube as a whole, wherein the reacting slurry driven by a recycling pump circulates with high-recycle rates, as depictured in Fig. 1. Under these conditions, it is possible and reasonable to assume the tubular loop reactor as a continuous stirred-tank reactor (CSTR) with constant volume [2,15,20,21], but slurry density. The reacting slurry is supposed to be a mixture of liquid phase (monomer and hydrogen) and a solid phase (polymer and catalyst). Finally, the catalyst is assumed to undergo the common activation–polymerization–decay pathway.

3. Mathematical model

3.1. Introduction

During the solid-catalyzed liquid-phase propylene polymerization in the tubular loop reactors, the small catalyst particles are continuously fed into R200 at a constant rate. The catalyst fragments into a large number of small particles or layers under mild reaction conditions in R200 [22], accordingly, the polymerization reaction is initiated, and the catalyst particles are well filmed to prevent the fragments from separating from the catalyst particles. Subsequently, the small catalyst particles coated with the thin

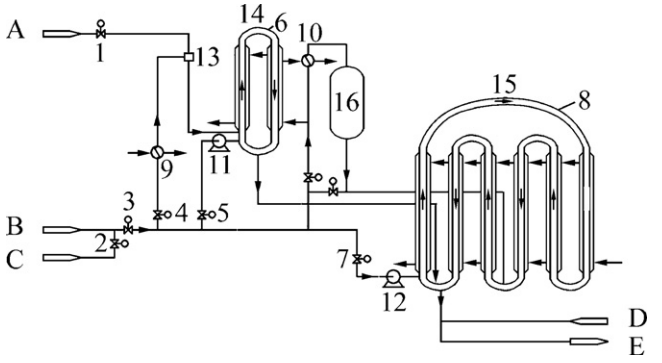

Fig. 1. Himont Spheripol Loop process (Fujian Petrochemical Company of SINOPEC): A—catalyst; B—propylene; C—hydrogen; D—coolant in; E—coolant out; 1–8—control sites; 9—E201, heat exchanger; 10—E203, heat exchanger; 11—P200, pump; 12—P201, pump; 13—Z203, mixer; 14—R200, prepolymerization reactor; 15—R201, main polymerization reactor; 16—D202, buffer tank.

polymer film in R200 are transported into R201 and react with the incoming monomers. Simultaneously, the particles may either grow in size due to the polymerization reaction or rupture into small ones caused by mechanical or rheological attrition. Therefore, the polymer particle is influenced by the original size of the catalyst particle, the polymerization rate, the attrition rate, and the residence time [15]. Moreover, due to the original catalyst PSD and residence time distribution (RTD) inside the reactors, the final product PSD can be very broad. Accordingly, the population balance model should take into account of the following three basic aspects, namely, the propylene polymerization kinetics, the particle dynamics and the residence time distribution.

In the present study, attention is specially paid to the particle size of the solid phase. For the sake of simplicity, the polymer particle is assumed to be of spherical shape with constant density. According to Refs. [4,23], the polymer PSD in the reactors (R200 and R201) can be described via the statistical density function, $P(D)$, which can be formulated with the following equation:

$$\int_{D_{\min}}^{D_{\max}} P(D)\,\mathrm{d}D = 1 \tag{1}$$

where $P(D)\,\mathrm{d}D$ is the mass fraction of the polymer particles in the size range of $(D, D+\mathrm{d}D)$. Note that due to the well-mixed assumption for the particles in the reactors, the particle density function in the product steam is identical to that in the reactors.

3.2. Polymerization kinetics

To describe the propylene polymerization kinetics over a Ziegler–Natta catalyst, a simple kinetic model is employed [6,24]. The polymerization kinetic scheme comprises a series of elementary reactions, namely, site activation, propagation, site deactivation, site transformation and chain transfer reactions. Among them, the propagation reaction and the site deactivation play an important role in the particle growth rate [6,22]. Based on the above discussion and the pseudo-kinetic rate constant method, the following kinetic equations are suggested and adopted:

- Propagation rate:

$$r_p = k_p M c^* M_m \tag{2}$$

- Site deactivation rate:

$$r_d = k_d c^* \tag{3}$$

Combination of Eqs. (2) and (3) leads to

$$r_d = -\frac{\mathrm{d}c^*}{\mathrm{d}t} = k_d\left(\frac{r_p}{k_p M \cdot M_m}\right) \tag{4}$$

Integrate r_p with the isothermal condition and r_p as a function of time, t, thus Eq. (5) can be obtained:

$$r_p = r_{p,0}\,\mathrm{e}^{-k_d t} \tag{5}$$

where it is important to point out that the feed impurity can lead to the catalyst deactivation. Besides, the catalyst can also deactivate spontaneously [3]. Therefore, k_d is supposed to represent the above two deactivation routes totally, which are independent and dependent, respectively.

When referring to the polymer particles, the inter- and intra-particle heat and mass transfer limitations do affect the polymerization rate. Though slow reaction rate considered in Ref. [25], some aspects of polymer particle's growth are similar, thus we assume that the polymerization rate are more likely to be affected by the amount of the polymer produced on the surface of the catalyst particle compared with the residence time in the early stage of polymerization. Thus, Eq. (5) can possibly be improved and modified empirically as shown below:

$$r_p(t) = \eta \cdot \left(\frac{D_{cat}}{D_{pp}}\right)^n \mathrm{e}^{-k_d t} \cdot r_{p,0} \tag{6}$$

wherein D_{cat} and D_{pp} are the catalyst and the polymer particle diameter, respectively; η represents the efficiency factor, which is a liner function of D_{cat} shown in Eq. (7), describing the specific surface and the active sites buried in the support material of different size. Notice that D_{pp} is also a function of the residence time and the catalyst particle diameter D_{cat}, which is described in Eq. (8):

$$\eta = -k_e \cdot D_{cat} + 1 \tag{7}$$

$$D_{pp} = D_{pp}(t, D_{cat}) \tag{8}$$

3.3. Particle dynamics

According to Refs. [2,3,5,6,13,15], the following assumptions for particle dynamics are made in this paper:

(1) all catalyst active sites have been activated simultaneously,
(2) there are no radial concentration gradients within the particles,
(3) the temperature gradients in the particles are ignored.

Assuming a polymer particle formed base on a catalyst particle, then the following mass balance equation can be obtained:

$$\frac{\pi}{6} D_{cat}^3 \rho_{cat} \int_0^t r_p(t)\,\mathrm{d}t = \frac{\pi}{6}(D_{pp}^3 - D_{cat}^3)\rho_{pp} \tag{9}$$

In addition, Eq. (10) can be obtained via derivation of Eq. (9):

$$r_p(t) = \left(\frac{3\rho_{pp} \cdot D_{pp}^2}{\rho_{cat} \cdot D_{cat}^3}\right)\frac{\mathrm{d}D_{pp}}{\mathrm{d}t} \tag{10}$$

Based on the constant value of D_{cat} for a single polymer particle, the correlation of D_{pp} and t can also be obtained and shown in Eq. (11) by incorporating Eq. (6) into Eq. (10):

$$\eta \cdot \left(\frac{D_{cat}}{D_{pp}}\right)^n \mathrm{e}^{-k_d t} \cdot r_{p,0} = \left(\frac{3\rho_{pp} \cdot D_{pp}^2}{\rho_{cat} \cdot D_{cat}^3}\right)\frac{\mathrm{d}D_{pp}}{\mathrm{d}t} \tag{11}$$

Accordingly, Eqs. (12) and (13) can be obtained by integrating Eq. (11):

$$D_{pp} = D_{pp}(t, D_{cat}) = \left[\frac{(3+n)\cdot\eta\cdot r_{p,0}\cdot\rho_{cat}\cdot D_{cat}^{(3+n)}\cdot(1-\mathrm{e}^{-k_d t})}{3\cdot\rho_{pp}\cdot k_d} + D_{cat}^{(3+n)}\right]^{1/(3+n)} \tag{12}$$

$$t = t(D_{pp}, D_{cat}) = \frac{1}{k_d}\ln\left[1 - \frac{3(D_{pp}^{3+n} - D_{cat}^{3+n})\cdot\rho_{pp}\cdot k_d}{(3+n)\cdot\eta\cdot r_{p,0}\cdot\rho_{cat}\cdot D_{cat}^{3+n}}\right] \tag{13}$$

From the viewpoint of statistical methodology, it is obvious that a polymer particle with diameter of D_{pp} in the size range of (D_i, D_{i+1}) has the following possibility:

$$\int_{D_i}^{D_{i+1}} P_{pp}(D_{pp})\,\mathrm{d}D_{pp} = \int_{D_{cat,\min}}^{D_{cat,\max}} \int_{t_i^j}^{t_{i+1}^j} E_{pp}(t)\,\mathrm{d}t \cdot P_{cat}(D_{cat})\,\mathrm{d}D_{cat} \tag{14}$$

where $P_{cat}(D_{cat})$ is the catalyst PSD density function; $E_{pp}(t)$ is the residence time distribution based on the polymer particles for each diameter of catalyst particles; t_i^j and t_{i+1}^j are both functions of D_{pp}

and D_{cat} as discussed in Eq. (13). In addition, as for the discrete situation, Eq. (14) can be rewritten as Eq. (15):

$$W_{pp,i} = \sum_{j=1}^{n_{cat}} m_{cat,j} \cdot \int_{t_i^j}^{t_{i+1}^j} E_{pp}(t)\,dt \tag{15}$$

where n_{cat} represents the number of catalyst particle diameter size cuts; $m_{cat,j}$ represents the mass fraction of catalyst particles in each size cuts; $W_{pp,i}$ represents the mass fraction of polymer particles with the diameter lying between D_i and D_{i+1}.

For the sake of estimation for kinetic parameters from plant data, a chi-square merit function is defined and used to determine best-fit parameters by its minimization:

$$\chi^2 = \sum_{i=1}^{n_{pp}} \left(\frac{W(D)_{pp,i} - \hat{W}(D)_{pp,i}}{\sigma(D)_i} \right) \tag{16}$$

where n_{pp} is the number of plant data points and $\sigma(D)$ is the standard deviation of the plant data points [26].

3.4. Steady-state population balance model

3.4.1. Particle growth and attrition

For the sake of the simplicity and keeping in consistence with the particle dynamics presented above, a simplification of the morphology model is introduced and the growth rate of the polymer particle diameter is given as follows, which is derived from Eq. (10) [4,8]:

$$G(D) = \left(\frac{dD_{pp}}{dt} \right)_g = \frac{r_p(t) \cdot D_{cat}^3 \cdot \rho_{cat}}{3\rho_{pp} \cdot D_{pp}^2} \tag{17}$$

Mattos et al. [15] and Freitas et al. [27] assumed and testified, respectively, that particle coalescence and breakage were not important for PSD evolution in liquid-phase polymerization reactors. However, polymer particle attritions may occur under the conditions of high density and relatively fast circular velocity in the tubular loop reactors. Then, polymer fines may generate due to the attrition forces resulting from particle collision in the reactors, and actually, large amount of fines are found in the local plant. Under the assumption of a continuous size reduction of the polymer particles [23], the size of the subtle product can be considered to be infinitely small, accordingly, the amount of active sites contained can be ignored. Thus, the subtle product attrited makes little contribution to the overall polymerization rate [4]. Denoting $R_a(D)$ as the particle attrition rate, the average rate of particle mass change per particle mass due to the attrition can be described in Eq. (18):

$$\frac{(dm_{pp}(D_{pp})/dt)}{m_{pp}(D_{pp})} = \frac{3R_a(D_{pp})}{D_{pp}} \tag{18}$$

3.4.2. Formulation of population balance equation

Following the population balance method described in Fig. 2 [4], the steady-state mass balance equation for particles in the size range of $(D, D + \Delta D)$ is given by Eq. (19):

{Particle entering with catalyst feed} {Particle leaving in the product} + {Particle entering the interval from a smaller size due to polymerization}

{Particle leaving the interval to a larger size due to polymerization} + {Particle entering the interval from larger size due to attrition} {Particle leaving the interval to a smaller size due to attrition}

+ {Generation of particle mass within the interval due to polymerization} {Loss of particle mass within the interval due to attrition} = 0 (19)

It is necessary to mention that for a particle size distributed feed, the first term in Eq. (19) represents the particle inflow in the size range of $(D, D + \Delta D)$, which is the case of R201 when the outflow of R200 enters into with size-distributed polymer particles. On the other hand, for a uniform-size catalyst feed as in R200, this term is only taken into account for the first particle cut. Substitute each of the related terms in Eq. (19) for mathematical expression using the particle density function, particle growth rate and attrition rate, as well as the corresponding mass flow rate, then we obtain:

$$\left(\frac{F_1}{W}\right) P_1(D_i)\,\Delta D - \left(\frac{F_2}{W}\right) P_2(D_i)\,\Delta D + P_2(D_{i-1}) G(D_{i-1}) + P_2(D_{i+1}) R_a(D_{i+1}) + P_2(\overline{D_i}) \frac{3G(\overline{D_i})}{\overline{D_i}}\,\Delta D - P_2(D_i)(G(D_i) + R_a(D_i)) - P_2(\overline{D_i}) \frac{3R_a(\overline{D_i})}{\overline{D_i}}\,\Delta D = 0 \tag{20}$$

All of the terms of Eq. (20) are divided by ΔD and let ΔD approaches to 0; accordingly, the continuous form of the population balance equation for the case of uniform-size catalyst feed is obtained as given below:

$$\left(\frac{F_1}{W}\right) P_1(D) - \left(\frac{F_2}{W}\right) P_2(D) - \frac{d}{dD}[P_2(D)G(D)] + \frac{d}{dD}[P_2(D)R_a(D)] + P_2(D)\frac{3}{D}[G(D) - R_a(D)] = 0 \tag{21}$$

According to Ref. [4], when catalyst particles of size D_{cat} enter into a loop reactor, once they get contact with the liquid phase monomer, polymerization occurs and their sizes increase instantaneously by at least a very small increment before they exit the reactor. Therefore, the particle size distribution appears to be discontinuous at $D_{pp} = D_{cat}$, or otherwise:

$$P_{pp}(D) = \begin{cases} 0 & D_{pp} = D_{cat} \\ P_{pp}(D_0) & D_{pp} = D_0 \end{cases} \tag{22}$$

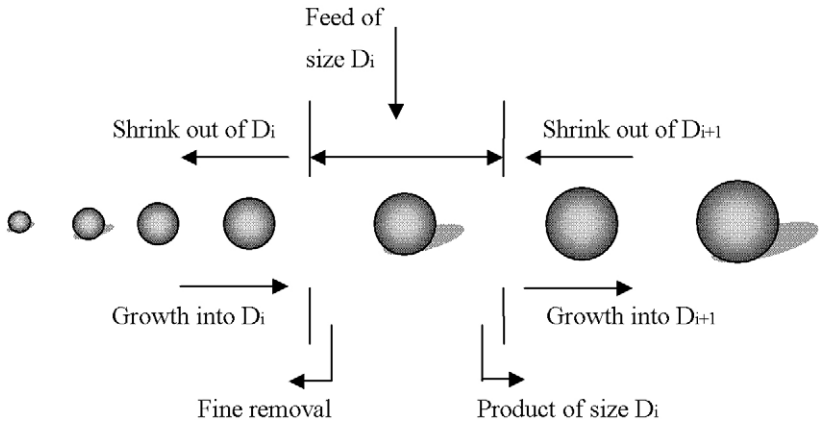

Fig. 2. Schematic representation of particle size variation with respect to particle growth and attrition mechanism.

where D_0 is an arbitrary value close to D_{cat}, but not exactly equals to D_{cat}. For the case of size distributed catalyst feed, the particle density function will be given by the weighted integral of the particle size distributions resulting from the various discrete uniform size catalyst fractions:

$$P_{pp}(D_{pp}) = \int_{D_{cat,\min}}^{D_{cat,\max}} P_{pp}(D_{pp}, D_{cat}) P_{cat}(D_{cat})\, \mathrm{d}D_{cat} \tag{23}$$

3.5. Solution methodology

The present study has considered R200 and R201 as shown in Fig. 1. The corresponding solution methodology is introduced as follows.

First, the input is read through the Read Input module. The input is validated and the initialization of the model variables is done. The overall reactors (R200, R201) simulation is calculated in the external Reactors Module (not discussed in this paper). This external module is incorporated to supply the total particle mass, W; the polymer particles output rate, F_1 and F_2, in the tubular loop reactors as expressed in Eq. (21), besides, the polymer properties including the molecular weight distribution and melt index. For more information, readers are encouraged to refer Refs. [1,12,28]. According to the external module, we can easily predict both the polymer PSD and properties, and discuss the effects of the operational parameters on the polymer PSD. Then the program goes to the next modules solving the population balance equations for R200 and R201, in sequence. To solve these steady-state population balance equations, shown in Eq. (21), the whole range of variation of particle diameter is divided into a suite of equally spaced diameters. Subsequently, the differential Eq. (21) is approximated by a system of linear recursive algebraic equations written at discrete diameters, and then this system of linear algebraic equations is recursively solved for each catalyst diameter cuts starting from each catalyst size, to calculate the PSD in the reactors in sequence [4]. It is important to point out that in present study, $P_{pp}(D_0)$ is rearranged to make Eqs. (1) and (23) satisfied. This procedure is different from Refs. [4,8], wherein the value of the product outflow rate is rearranged to make Eqs. (1) and (23) satisfied given the case of the constant bed weight in the FBR. Herein, the two PSDs of the two reactors have been calculated; moreover, if plant data are available, it is interesting that the selective route of parameters estimating can be chosen to estimate k_d, k_e and n introduced previously. Besides, there is a 'RTD for polymer' module wherein the polymer particles' residence time distribution is obtained by introducing Eq. (13) and (24):

$$E_{pp}(t) = \frac{\mathrm{d}F_{pp}(t)}{\mathrm{d}t} = \frac{\mathrm{d}\left(\int_0^t P_{pp}[D_{pp}(t, D_{cat})] \cdot (\mathrm{d}D_{pp}/\mathrm{d}t)\,\mathrm{d}t\right)}{\mathrm{d}t} \tag{24}$$

Because of the catalyst's short residence time in R200 and its mild reaction conditions, there is only a little effect of the R200 on the total polymer PSD, thus, in the estimation procedure, only R201 is taken into account. With the residence time distribution of the polymer particles in the tubular loop reactors and the plant data including PSDs of the polymer and catalyst, the kinetic parameters of k_d, k_e and n can be fitted iteratively through the procedure discussed in Section 3.3. On the one hand, the estimation procedure is necessary when lots of parameters are to be confirmed or sorts of parameters are available; on the other hand; we also emphasize that the catalyst, especially, its support material have important effects on the catalyst fragmentation and the intra-particle mass and heat limitations. Papers published on the polymer particles and catalyst fragmentations have clearly shown the importance of the support material of the catalyst [25]. Therefore, it is necessary to describe an empirical single polymer particle model as accurate as possible through parameter estimation.

4. Results and discussion

4.1. Parameters estimation

The catalyst used in the plant is an advanced fourth generation of the Ziegler–Natta catalyst ($TiCl_4/MgCl_2$ + PEEB + AlR_3), and was sampled and characterized by means of microscope to obtain the particle accumulation curve, and then the particle density curve was also obtained by derivation. Both the corresponding curves are shown in Fig. 3. The polymer powder obtained from the plant was analyzed by using a sizer and was also numerically tackled, the same as the catalyst, and the result is given in Fig. 4.

The estimation of kinetic parameters was accomplished as discussed in Section 3.5 using the above plant data. Accordingly, the values of k_d, k_e and n were obtained successfully. Moreover, according to the value of k_d, the value of $k_{d,0}$ is also updated via the Arrhenius law. It can be seen from Fig. 5 that the predicted data is in good agreement with the plant data. Hence, the single particle model was available as accurate as possible with updated kinetic parameters through estimation procedure. Parts of parameters estimated or used here are tabulated in Table 1. The following shows the employment of this single particle model.

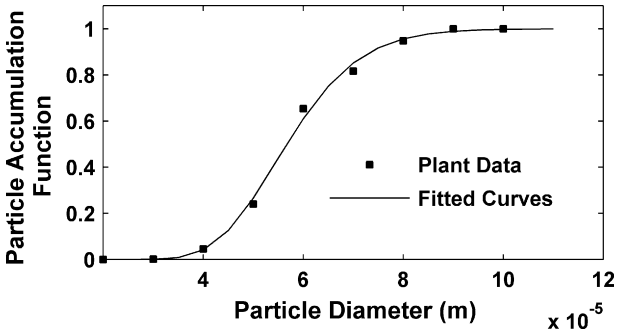

Fig. 3. Catalyst PSD from Plant.

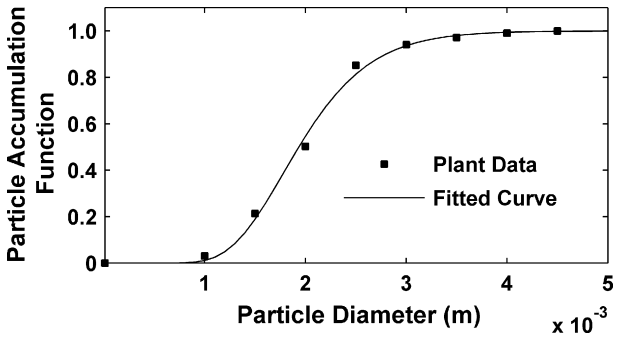

Fig. 4. Polymer PSD from Plant.

As shown in Fig. 6, the polymerization rate decreases greatly in the initial stage of polymerization due to the strong decrease of D_{cat}/D_{pp} ratio in the early stage of the polymer/catalyst particle formed. For catalyst particles with different efficiency factor η according to Eq. (7), the polymerization rate decays according to the corresponding initial polymerization rate. Pater et al. [25] have put forward an argument that the above result is ascribed to the phase transition in the growing particle. That it is, initially, the catalyst forms the continuous phase, within which the polymer is distributed. Then after the phase transition, the polymer forms the continuous phase in which catalyst fragments are distributed. And this change causes a change in monomer concentration at the active sites, resulting in lower reaction rates. Besides, Hutchinson et al. [29] also notice the difference of the monomer concentration between the active site and the bulk fluid-phase.

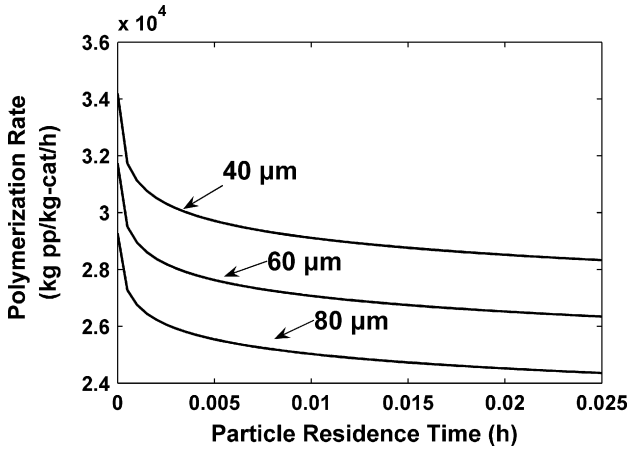

Fig. 6. Polymerization rate decays with time at the initial stage of polymerization.

Table 1
Simulated parameters in the study.

Parameter	Value	Unit	Ref.
E_p	5.04×10^4	J/mol	[1,28]
E_d	5.04×10^4	J/mol	[1,28]
$k_{p,0}$	1.789×10^8	$m^3/(mol\,h)$	[1,28]
$k_{d,0}$	6.313×10^5	h^{-1}	Estimated
k_e	3.15×10^3	m^{-1}	Estimated
n	9.1264×10^{-2}	–	Estimated
C^*	25	mol/kg-cat	Plant data
ρ_{pp}	910	kg/m^3	Plant data
ρ_{cat}	600	kg/m^3	Plant data

Fig. 7 shows the polymerization rate of different catalyst particles decays in same trend as a whole. That it is, all polymerization rates first decay strongly in the small diameter range due to the mass or heat limitations, and then decrease gently for a short residence time before the polymerization rates decay severely due to the active site deactivation in the large diameter range, namely, the long residence time in the reactors. Besides, it is important to point out that catalyst particles with different diameters take different residence time to reach the same diameter.

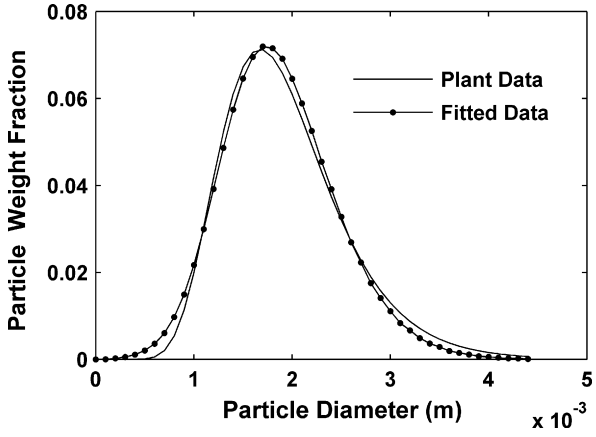

Fig. 5. Comparison of the particle weight fraction between the predicted data and the plant data.

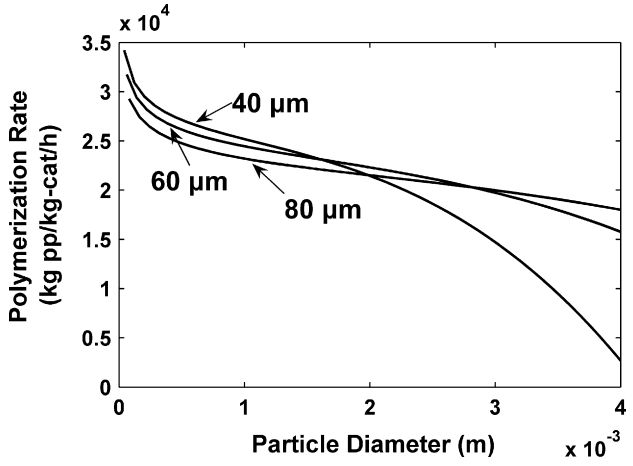

Fig. 7. Polymerization rate decays with particle growth.

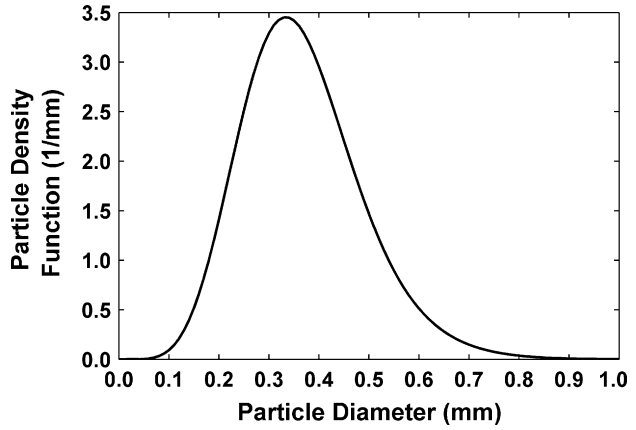

Fig. 8. Particle size distribution predicted for R200: T_{200} = 15.5; T_{201} = 70; F_{TEAL} = 3.37; F_{DONOR} = 0.33; F_{cat} = 0.5775; F_{H_2} = 0.7; F_{prop} = 24616.14; $F_{prop,200}$ = 1500.03.

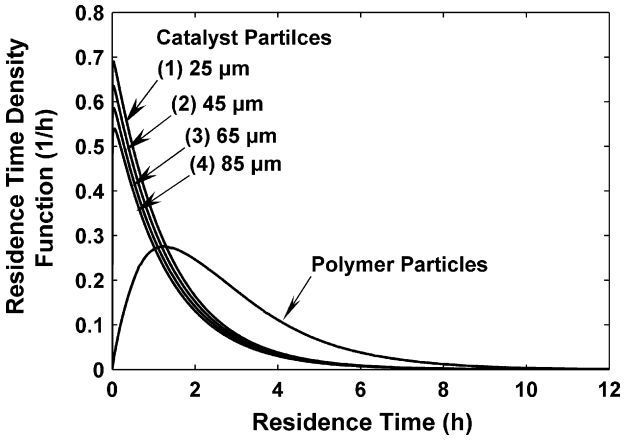

Fig. 10. Residence time distribution for the catalyst and polymer particles.

4.2. Comparison between the plant data and the simulated data

The polymer PSD data predicted by the population balance model are compared with the plant data. Because the R200 reactor is relatively small in volume and the corresponding polymerization rate is also small with its mild conditions. In addition, the polymer particles in R200 are difficult to sample. Therefore, only the polymer particles in R201 were sampled and their PSD data are used in present study, but both of the PSDs predicted of the two reactors are shown in Figs. 8 and 9.

Fig. 9 shows that there is a very good agreement between the predicted data and the plant data. Therefore, the present work can be applied to predict the polymer PSD in the steady-state tubular loop reactors; though Fig. 9 shows that the predicted data has more fine powder and less large particles than the plant data. The reasons for these differences may be the neglects of the agglomeration effect during the polymerization and the electrostatic effect during the experimental analysis of the polymer samples, which may alter the shape of the PSD more or less. What's more, the assumption of well mixed in tubular loop reactor also affects on the predicted results.

For polymer particles with diameter of D_{pp} in a size cut of dD_{pp}, their total mass can be expressed in Eq. (25), where $E_{cat}(t)$ is the residence time distribution based on the catalyst. By incorporating Eq. (12) into Eq. (25), the residence time distribution for the catalyst particles can be obtained and shown in Eq. (26):

$$W \cdot P_{pp}(D_{pp})\,dD_{pp} = \left(\frac{\pi}{6}D_{pp}^3\rho_{pp} - \frac{\pi}{6}D_{cat}^3\rho_{cat}\right) \cdot \frac{F_{cat}\cdot E_{cat}(t)\,dt}{(\pi/6)D_{cat}^3\rho_{cat}} \tag{25}$$

$$E_{cat}(t) = \frac{W \cdot D_{cat}^3\rho_{cat}}{(D_{pp}^3\rho_{pp} - D_{cat}^3\rho_{cat})F_{cat}} \frac{dD_{pp}}{dt} \cdot P_{pp}(D_{pp}) \tag{26}$$

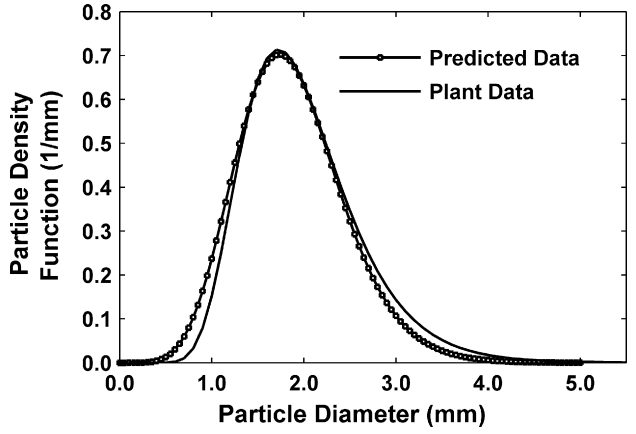

Fig. 9. Comparison between the predicted data and the plant data: T_{200} = 15.5; T_{201} = 70; F_{TEAL} = 3.37; F_{DONOR} = 0.33; F_{cat} = 0.5775; F_{H_2} = 0.7; F_{prop} = 24616.14; $F_{prop,200}$ = 1500.03.

Based on the population balance equations for uniform-size catalyst feed, residence time distributions for some of the catalyst cuts are shown in Fig. 10. In addition, the residence time distributions of the polymer particles discussed previously are also shown in Fig. 10, which are all identical for each of the catalyst cuts. Fig. 10 shows that the residence time distributions of the polymer and the catalyst are different even though they are both suspending in the liquid phase and dragged through the tubular loop reactors with the liquid phase. The reason for this difference is that the polymer particles grow with the increase of the residence time but the catalyst particles remains constant in mass with the polymerization continuing. Therefore, the residence time distribution of the catalyst seems to the same as that of the liquid phase, which assumed as the perfect mixed.

In addition, Fig. 10 also shows that catalyst particle with different size has different residence time distribution, and the above difference is caused by Eq. (21), wherein, for each single-size catalyst feed, the weight of the total solid in the reactor, W, resulting from the external module, remains constant, but each catalyst particle is different in polymerization rate. Thus, to reach the same W, the residence time for larger catalyst particles have to be extended according to Eq. (7).

It's interesting that the population balance model proposed here and the models proposed by Zacca et al. [2] concerning the loop reactor both characterize the catalyst's residence time distribution as the type of CSTR.

4.3. Single-size catalyst feed

4.3.1. Effects of the feed catalyst size on the polymer PSD

The effects of the feed catalyst particle size on the polymer PSD are shown in Figs. 11 and 12, which show that the average diameter of the polymer particles increases and there is a clear shift to broader PSD with the increase of the diameter of the catalyst particles. The increase of the reaction rate at larger catalyst leads to

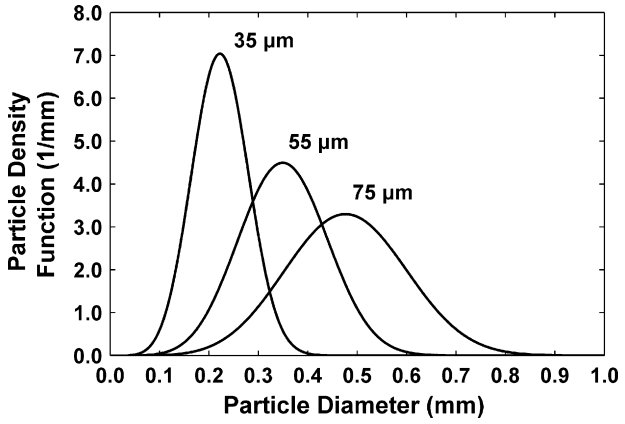

Fig. 11. Effects of the catalyst size on the polymer PSD in R200: T_{200} = 15.5; T_{201} = 70; F_{TEAL} = 3.37; F_{DONOR} = 0.33; F_{cat} = 0.5775; F_{H_2} = 0.7; F_{prop} = 24616.14; $F_{prop,200}$ = 1500.03.

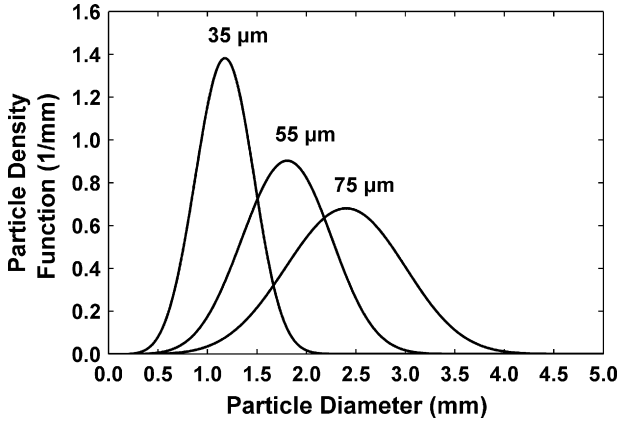

Fig. 12. Effects of the catalyst size on the polymer PSD in R201: T_{200} = 15.5; T_{201} = 70; F_{TEAL} = 3.37; F_{DONOR} = 0.33; F_{cat} = 0.5775; F_{H_2} = 0.7; F_{prop} = 24616.14; $F_{prop,200}$ = 1500.03.

the increase of the polymer particle's diameter, and it's also well explained according to Eq. (17).

4.3.2. Effects of the polymerization parameters on the polymer PSD

For propylene polymerization in industry, the polymer PSD is affected by the polymerization parameters including the catalyst deactivation constant and the attrition rate constant.

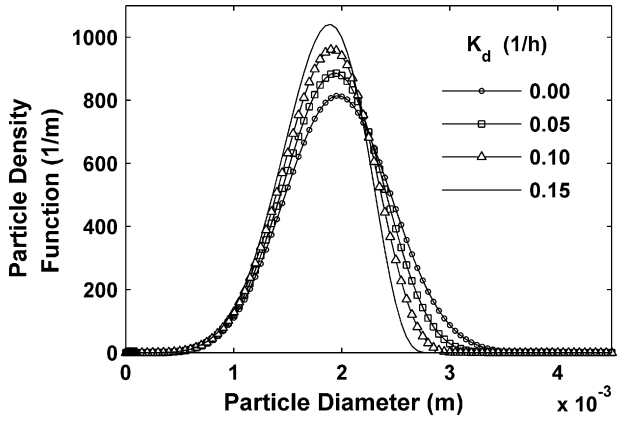

Fig. 13. Effects of the catalyst deactivation constant on the polymer PSD in R201: T_{200} = 15.5; T_{201} = 70; F_{TEAL} = 3.37; F_{DONOR} = 0.33; F_{cat} = 0.5775; F_{H_2} = 0.7; F_{prop} = 24616.14; $F_{prop,200}$ = 1500.03.

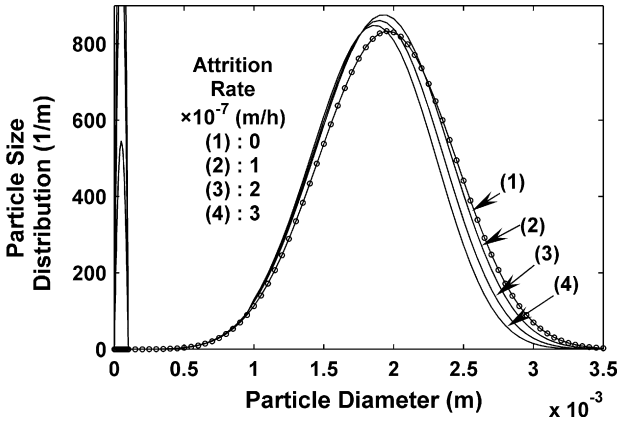

Fig. 14. Effects of the attrition rate constant on the polymer PSD in R201: T_{200} = 15.5; T_{201} = 70; F_{TEAL} = 3.37; F_{DONOR} = 0.33; F_{cat} = 0.5775; F_{H_2} = 0.7; F_{prop} = 24616.14; $F_{prop,200}$ = 1500.03.

Fig. 13 illustrates the effect of the catalyst deactivation constant on the polymer PSD in R201. For first-order site deactivation kinetics and a given catalyst feed rate, the active site concentration in the polymer particles decreases greatly with the increase of the deactivation rate constant. Accordingly, the polymerization rate decreases with the particles' residence time and the polymer PSD curves become sharp in large particles. Fig. 13 shows that for faster deactivation constant, the product PSD shifts to lower particle size.

Figs. 14 and 15 show the effects of the attrition rate constant on the polymer PSD. Unlike previously published work [4]; the attrition rate is redefined in Eq. (27):

$$R_a = \begin{cases} 0 & D_{pp} < 1\,\text{mm} \\ \left(\dfrac{w}{0.55}\right) \times 10^{-7} & D_{pp} \geq 1\,\text{mm} \end{cases} \quad (27)$$

where the attrition rate of polymer particles in the diameter range of 0–1 mm is assumed to be 0, and w is the weight fraction of the solid phase in the reactor. It suggests that when the density of the material within the loop reactor gets higher, the attrition rate will increase, so does the fine powder.

According to Ref. [30], the particle size distribution of the polymer fines, given in Eqs. (28)–(30) in the reactor and outflow streams

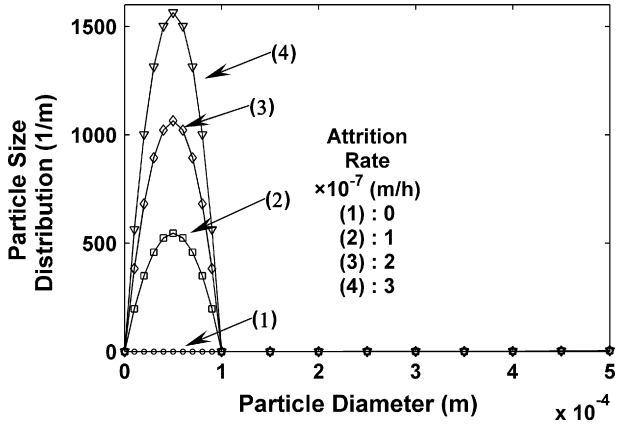

Fig. 15. Fine powders produced with the increase of the attrition rate: T_{200} = 15.5; T_{201} = 70; F_{TEAL} = 3.37; F_{DONOR} = 0.33; F_{cat} = 0.5775; F_{H_2} = 0.7; F_{prop} = 24616.14; $F_{prop,200}$ = 1500.03.

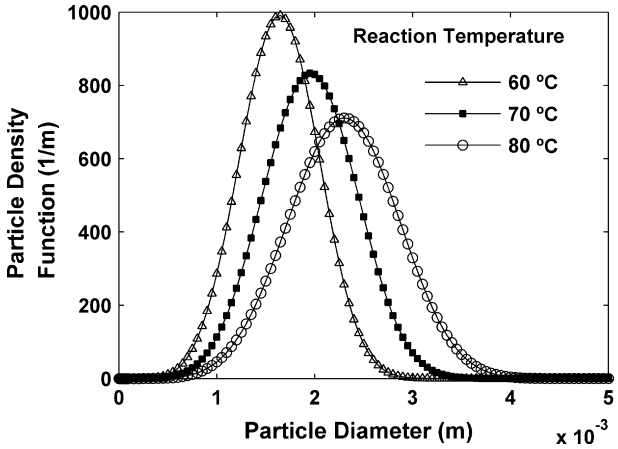

Fig. 16. Effects of the reaction temperature on the polymer PSD in R201: T_{200} = 15.5; F_{TEAL} = 3.37; F_{DONOR} = 0.33; F_{cat} = 0.5775; F_{H_2} = 0.7; F_{prop} = 24616.14; $F_{prop,200}$ = 1500.03.

are improved by following a conic function other than a delta function:

$$\int_{D_{f\min}}^{D_{f\max}} F_2 P_{pp}(D_f)\,\mathrm{d}D_f = \sum_{i=1}^{n_p} W \cdot P_{pp}(D_{pp}) \frac{3R_a(D_{pp,i})}{D_{pp,i}}\,\mathrm{d}D_{pp} \tag{28}$$

$$P_{pp}(D_f) = -A(D_f - D_{fmin})(D_f - D_{f\max}) \tag{29}$$

$$D_{f\min} \le D_f \le D_{f\max} \tag{30}$$

With the attrition rate constant increases, the polymer PSD becomes narrower and the weight fraction of the larger particles decreases slightly as showed in Fig. 14, though the fine powders increase evidently in Fig. 15.

4.3.3. Effects of the operational parameters on the polymer PSD

For propylene polymerization in industry, the polymer PSD is influenced by the polymerization temperature, the catalyst feed rate, and the propylene feed rate generally. These influences are predicted in our work.

Fig. 16 illustrates the effect of the liquid-phase polymerization temperature on the polymer PSD in R201. As can be seen from Fig. 16, the distribution width of the polymer PSD increases with the increase of the polymerization temperature in R201. Simultaneously, there is a great shift in the PSD curve to larger polymer particles with the increase of the polymerization temperature. The observed shift of the PSD curve to large particles is due to the increase of the polymerization rate at high temperature.

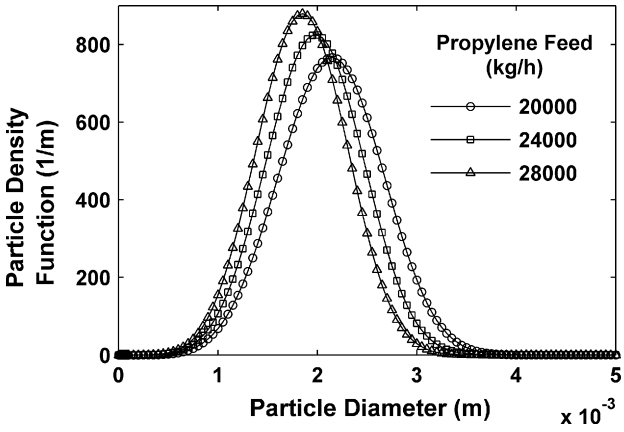

Fig. 18. Effects of the propylene feed rate on the polymer PSD in R201: T_{200} = 15.5; T_{201} = 70; F_{TEAL} = 3.37; F_{DONOR} = 0.33; F_{cat} = 0.5775; F_{H_2} = 0.7; $F_{prop,200}$ = 1500.03.

Figs. 17 and 18 show the effects of the catalyst feed rate and the propylene feed rate on the polymer PSD in R201, respectively.

With the increase of the catalyst feed rate, the total polymerization rate increases. Hence, the content of the solid in the reactor increases, leading the increase of the density of the mixture in R201, thus, increase the particle residence time, though, this slightly affects the product PSD, as shown in Fig. 17. With the increase of the propylene feed rate, as can be seen from Fig. 18 the catalyst average residence time in R201 decreases greatly, which leads to the decrease of the average polymer particle size.

The effect of the polymer PSD in R200 on the polymer PSD in R201 is showed in Figs. 19 and 20. There is nearly the same polymer PSD in R201 showed in Fig. 20 even though three case of polymer particles feed with different PSD from R200 into R200. It proves that the effect of the polymer PSD in R200 on the polymer PSD in R201 is weak.

4.4. Multi-size catalyst feed

Based on the single-size catalyst feed model and Eq. (23), the effect of the catalyst PSD on the polymer PSD in R201 can also be obtained via the above model. In present study, the initial catalyst PSD is divided into a number of size cuts and the overall PSD in R201 is obtained as a sum of PSDs resulted from the individual

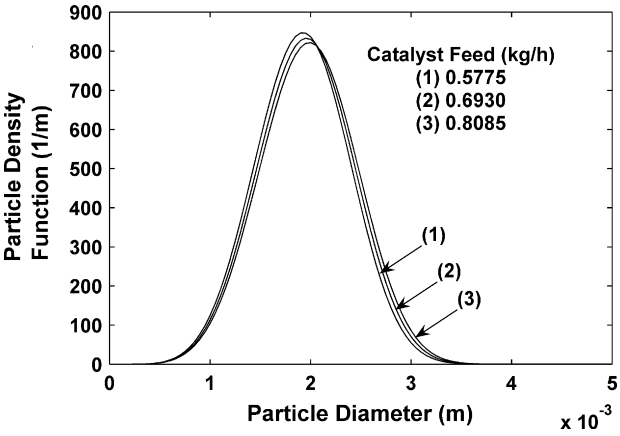

Fig. 17. Effects of the catalyst feed rate on the polymer PSD in R201: T_{200} = 15.5; T_{201} = 70; F_{TEAL} = 3.37; F_{DONOR} = 0.33; F_{H_2} = 0.7; F_{prop} = 24616.14; $F_{prop,200}$ = 1500.03.

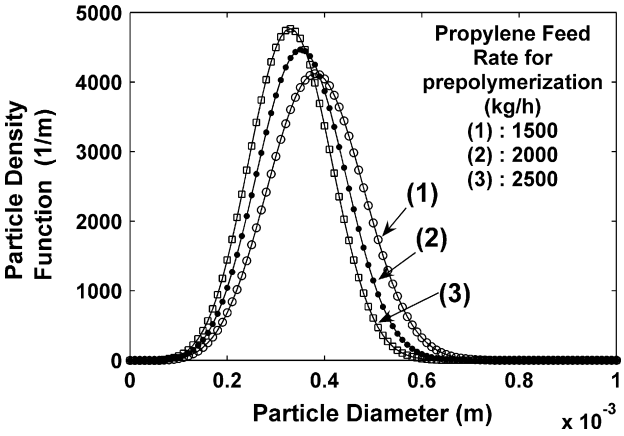

Fig. 19. Effects of the propylene feed rate on the polymer PSD in R200: T_{200} = 15.5; T_{201} = 70; F_{TEAL} = 3.37; F_{DONOR} = 0.33; F_{cat} = 0.5775; F_{H_2} = 0.7; F_{prop} = 24616.14.

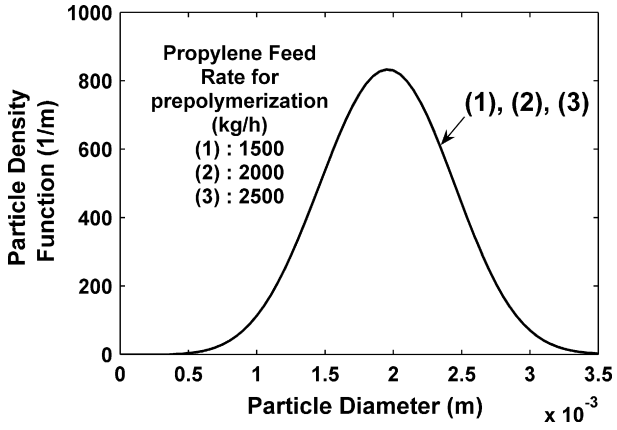

Fig. 20. Effects of the prepolymerization in R200 on main polymerization of R201: T_{200} = 15.5; T_{201} = 70; F_{TEAL} = 3.37; F_{DONOR} = 0.33; F_{cat} = 0.5775; F_{H_2} = 0.7; F_{prop} = 24616.14.

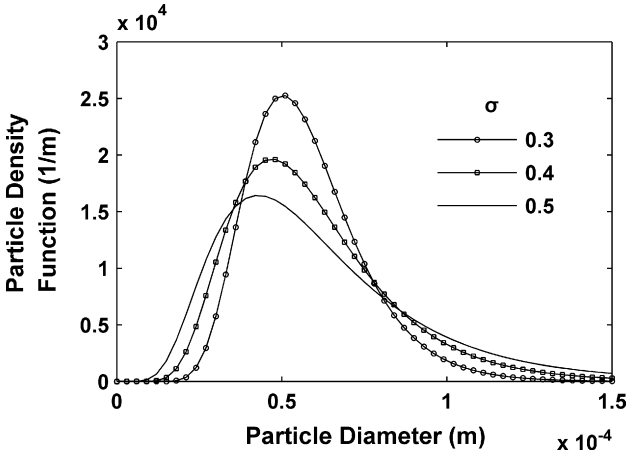

Fig. 21. Catalyst size distribution with different standard deviations.: T_{200} = 15.5; T_{201} = 70; F_{TEAL} = 3.37; F_{DONOR} = 0.33; F_{cat} = 0.5775; F_{H_2} = 0.7; F_{prop} = 24616.14; $F_{prop,200}$ = 1500.03.

catalyst cuts. Hatzantonis et al. [4] assumed that the feed catalyst PSD has a log-normal distribution and is shown in Eq. (31). Accordingly, the feed catalyst size distribution is illustrated in Fig. 21, and the corresponding predicted polymer PSD is also shown

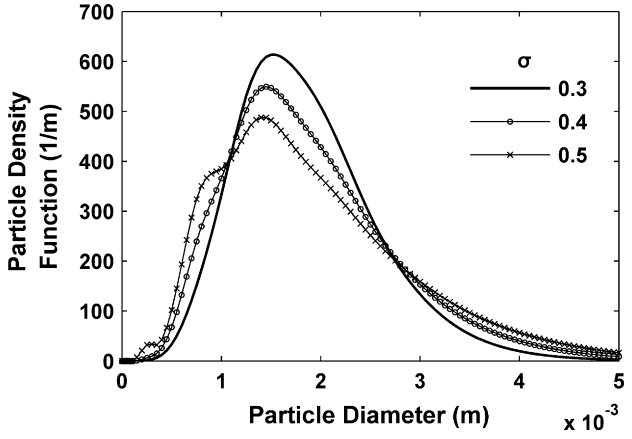

Fig. 22. Effects of catalyst size distribution on the PSD in R201: T_{200} = 15.5; T_{201} = 70; F_{TEAL} = 3.37; F_{DONOR} = 0.33; F_{cat} = 0.5775; F_{H_2} = 0.7; F_{prop} = 24616.14; $F_{prop,200}$ = 1500.03.

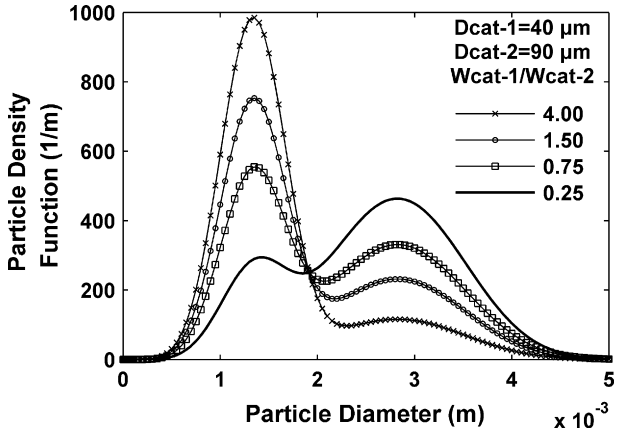

Fig. 23. Effects of the catalyst particle size multi-distribution on the polymer PSD in R201: T_{200} = 15.5; T_{201} = 70; F_{TEAL} = 3.37; F_{DONOR} = 0.33; F_{cat} = 0.5775; F_{H_2} = 0.7; F_{prop} = 24616.14; $F_{prop,200}$ = 1500.03.

in Fig. 22:

$$P_{cat}(D_{cat}) = \frac{1}{\sqrt{2\pi}D_{cat}\sigma}\exp\left(-\frac{(\ln D_{cat} - \ln \overline{D_{cat}})^2}{2\sigma^2}\right) \quad (31)$$

Fig. 21 shows that the three catalysts fed with the same $\overline{D_{cat}}$ of 60 μm are different in σ of 0.3, 0.4 and 0.5 based on Eq. (31). Moreover, the three corresponding polymer PSDs are also obtained via our model and illustrated in Fig. 22. In addition, Fig. 23 illustrates that the bimodal polymer PSD can be obtained by using a catalyst feed consisting of two types of catalyst particles with distinct diameter, and the shape of the overall polymer PSD directly depends on the diameter and mass fraction of the two catalysts. With the increase of the fraction of the large catalyst particles, the area of the large polymer particles increases in the outlet polymer PSD. Therefore, it is possible to produce special polymer particles with certain PSD type by varying the feed catalyst PSD.

5. Conclusions

A comprehensive steady-state population balance model is developed for the prediction of the polypropylene PSD produced in tubular loop reactors. The model takes into account the flow type, the polymer particle dynamics and the particle growth. Some actual data of the steady-state polymerization collected from a local plant are supplied to verify the model. The predicted polymer PSD produced under steady-state polymerization condition is found to agree well with the plant data.

The effects of the kinetic and operational parameters on the polymer PSD are also investigated. The simulated results show that the average diameter of the polymer particles increases and there is a shift to a broader PSD with the increase of the diameter of the catalyst particles when the single-size catalyst feeds. Moreover, as to the single-size catalyst applied, the polymer PSD becomes narrower with the increases of both the deactivation rate constant and the attrition rate, but becomes broader with the increase of the polymerization temperature. Simultaneously, we also find that the average diameter of the polymer particles decreases with the increase of the propylene feed rate. Furthermore, the simulated results show that a bimodal PSD can be obtained by using a catalyst feed consisting of two catalysts with distinct diameter, the shape of the overall polymer PSD directly depends on the diameter and the mass fraction of this two catalysts.

Acknowledgments

The authors thank National Natural Science Foundation of China (no. 20406016) for financial support and Fujian Petrochemical Company of SINOPEC for plant data and permission to publish it. Authors also thank the anonymous referees for comments on this manuscript.

References

[1] Z.H. Luo, Y. Zheng, Z.K. Cao, S.H. Wen, Mathematical modeling of the molecular weight distribution of polypropylene produced in a loop reactor, Polym. Eng. Sci. 47 (2007) 1643–1649.
[2] J.J. Zacca, J.A. Debling, W.H. Ray, Reactor residence time distribution effects on the multistage polymerization of olefins. I. Basic principles and illustrative examples, polypropylene, Chem. Eng. Sci. 51 (1996) 4859–4886.
[3] D.Y. Khang, H.H. Lee, Particle size distribution in fluidized beds for catalytic polymerization, Chem. Eng. Sci. 52 (1997) 421–431.
[4] H. Hatzantonis, A. Goulas, C. Kiparissides, A comprehensive model for the prediction of particle-size distribution in catalyzed olefin polymerization fluidized-bed reactors, Chem. Eng. Sci. 53 (1998) 3251–3267.
[5] H. Yiannoulakis, A. Yiagopoulos, C. Kiparissides, Recent developments in the particle size distribution modeling of fluidized-bed olefin polymerization reactors, Chem. Eng. Sci. 56 (2001) 917–925.
[6] M.H. Yogesh, P.U. Ranjeet, V.R. Vivek, A computational model for predicting particle size distribution and performance of fluidized bed polypropylene reactor, Chem. Eng. Sci. 59 (2004) 5145–5156.
[7] B.Z. Yang, J.D. Wang, Y.R. Yang, Polyethylene particle dynamics of gas phase ethylene polymerization in fluidized bed reactor, Petrochem. Technol. 33 (2004) 1130–1132 (in Chinese).
[8] B.Z. Yang, W. Jiang, J.D. Wang, Y.R. Yang, Simulation of particle size distribution in gas phase ethylene polymerization fluidized-bed reactor, J. Chem. Eng. Chin. Univ. 19 (2005) 461–467 (in Chinese).
[9] T.F. Mckenna, J. Dupuy, R. Spitz, Modelling of transfer phenomena on heterogeneous Ziegler catalysts: differences between theory and experiment, an introduction, J. Appl. Polym. Sci. 57 (1995) 371–384.
[10] T.F. Mckenna, J. Dupuy, R. Spitz, Modelling of transfer phenomena on heterogeneous Ziegler catalysts. Part 3. Modelling of intraparticle mass transfer resistance, J. Appl. Polym. Sci. 63 (1997) 315–322.
[11] Z.H. Luo, J. Li, X.L. Zhan, X.B. Yao, Monte Carlo simulation of solid phase graft polymerization of acrylic acid onto polypropylene, J. Chem. Eng. Jpn. 37 (2004) 737–743.
[12] Z.H. Luo, Z.K. Cao, Y.T. Su, Monte Carlo simulation of propylene polymerization. (I) Effects of impurity on propylene polymerization, Chin. J. Chem. Eng. 14 (2006) 194–199.
[13] K.Y. Choi, X. Zhao, S. Tang, Population balance modeling for a continuous gas phase olefin polymerization reactor, J. Appl. Polym. Sci. 53 (1994) 1589–1594.
[14] J.B.P. Soares, A.E. Hamielec, Effect of residence time distribution on the size distribution of polymer particles made with heterogeneous Ziegler–Natta and supported metallocene catalysts. A generic mathematical model, Macromol. Theor. Simul. 4 (1995) 1085–1104.
[15] A.G. Mattos Neto, J.C. Pinto, Steady-state modeling of slurry and bulk propylene polymerizations, Chem. Eng. Sci. 56 (2001) 4043–4057.
[16] Pdero Henrique Hermes Araujo, Jose Carlos de la Cal, Jose Maria Asua, Jose Carlos Pinto, Modeling particle size distritbution (PSD) in emulsion copolymerization reactions in a continuous loop reactor, Macromol. Theor. Simul. 10 (2001) 769–779.
[17] Z.H. Luo, Z.K. Cao, N.J. Zhu, an analysis on model of a loop reactor for polypropylene under a steady operating condition, J. Xiamen Univ. (Nat. Sci.) 44 (2005) 534–537 (in Chinese).
[18] K.Y. Choi, W.H. Ray, Recent developments in transition metal catalysed olefin polymerization—a sury. I. Ethylene polymerization, J. Macromol. Sci. C: Polym. Rev. 25 (1985) 1–55.
[19] K.Y. Choi, W.H. Ray, Recent developments in transition metal catalysed olefin polymerization—a sury. II. Propylene polymerization, J. Macromol. Sci. C: Polym. Rev. 25 (1985) 57–97.
[20] B. Cui, Q.R. Zhang, Y.N. Li, C.Q. Cao, Z.Y. Zhu, Modeling and parameter distributions in a loop reactor employed for propylene polymerization, Chem. Ind. Eng. 13 (1996) 1–8 (in Chinese).
[21] B. Cui, Q. Ma, C.Q. Cao, Z.Y. Zhu, Q.R. Zhang, J.Z. Liu, H.T. Wang, Kinetic characteristics of the tubular loop reactor for propylene polymerization, Chem. React. Eng. Technol. 12 (1996) 263–269 (in Chinese).
[22] T.M.P. Jochem, W. Gunter, W.P.M. van Swaaij, Polymerization of liquid propylene with a 4th generation Ziegler–Natta catalyst: influence of temperature, hydrogen and monomer concentration and prepolymerization method on polymerization kinetics, Chem. Eng. Sci. 57 (2002) 3461–3477.
[23] O. Levenspiel, D. Kunii, T. Fitzgerald, The processing of solids of changing size in bubbling fluidized beds, Powder Technol. 69 (1968) 87–96.
[24] M. Caracotsios, Theoretical modeling of Amoco's gas phase horizontal stirred bed reactor for the manufacturing of polypropylene resins, Chem. Eng. Sci. 47 (1992) 2594–2596.
[25] J.T.M. Pater, G. Weickert, J. Loos, W.P.M. van Swaaij, High precision propolymerization of propylene at extremely low reaction rates—kinetics and morphology, Chem. Eng. Sci. 56 (2001) 4107–4120.
[26] J.B.P. Soares, A.E. Hamielec, Deconvolution of chain-length distributions of linear polymers made by multiple-site-type catalyst, Polymer 11 (1995) 2257–2263.
[27] M.F. Freitas, Modelagem e Simulacao de Reatores de Polimerizacao de Etileno em Leito de Lama, DSc thesis, PEQ/COPPE, Universidade Federal do Rio de Janeiro, Rio de Janeiro, 1998.
[28] Y. Zheng, Modeling for Propylene Polymerization in a Liquid Phase Loop Reactor, Master Thesis, Xiamen University, P.R. China, 2006.
[29] R.A. Hutchinson, C.M. Chen, W.H. Ray, Polymerization of olefins through heterogeneous catalysis X: modeling of particle growth and morphology, J. Appl. Polym. Sci. 44 (1992) 1389–1414.
[30] T.P. Chen, S.C. Saxena, Solids population balance for attrition in fluidized beds, Powder Technol. 18 (1977) 279–281.